# Use of $\beta$3-methionine as an amino acid substrate of Escherichia coli methionyl-tRNA synthetase

Giuliano Nigro, Sophie Bourcier, Christine Lazennec-Schurdevin, Emmanuelle Schmitt, Philippe Marlière, Yves Mechulam

Journal of Structural Biology 209 (2020) 107435

Contents lists available at ScienceDirect

Journal of Structural Biology

journal homepage: www.elsevier.com/locate/yjsbi

# Use of $\beta^3$-methionine as an amino acid substrate of *Escherichia coli* methionyl-tRNA synthetase

Giuliano Nigro[a], Sophie Bourcier[b], Christine Lazennec-Schurdevin[a], Emmanuelle Schmitt[a,*], Philippe Marlière[c], Yves Mechulam[a,*]

[a] Laboratoire de Biochimie, BIOC, Ecole polytechnique, CNRS, Institut Polytechnique de Paris, 91128 Palaiseau Cedex, France
[b] Laboratoire de Chimie Moléculaire, LCM, Ecole polytechnique, CNRS, Institut Polytechnique de Paris, 91128 Palaiseau Cedex, France
[c] Xenome Research Group, Institute of Systems and Synthetic Biology, CNRS, UMR8030, UEVE, CEA, GENOPOLE, 5 rue Henri Desbruères, 91030 Evry Cedex, France

ARTICLE INFO

*Keywords:*
Non-standard amino acid
Beta amino acid
Translation
X-ray crystallography
tRNA aminoacylation

ABSTRACT

Polypeptides containing β-amino acids are attractive tools for the design of novel proteins having unique properties of medical or industrial interest. Incorporation of β-amino acids *in vivo* requires the development of efficient aminoacyl-tRNA synthetases specific of these non-canonical amino acids. Here, we have performed a detailed structural and biochemical study of the recognition and use of $\beta^3$-Met by *Escherichia coli* methionyl-tRNA synthetase (MetRS). We show that MetRS binds $\beta^3$-Met with a 24-fold lower affinity but catalyzes the esterification of the non-canonical amino acid onto tRNA with a rate lowered by three orders of magnitude. Accurate measurements of the catalytic parameters required careful consideration of the presence of contaminating α-Met in $\beta^3$-Met commercial samples. The 1.45 Å crystal structure of the MetRS: $\beta^3$-Met complex shows that $\beta^3$-Met binds the enzyme essentially like α-Met, but the carboxylate moiety is mobile and not adequately positioned to react with ATP for aminoacyl adenylate formation. This study provides structural and biochemical bases for engineering MetRS with improved $\beta^3$-Met aminoacylation capabilities.

## 1. Introduction

The design of polypeptides having enhanced or novel properties is a major challenge for synthetic biology. Indeed, although natural proteins mostly rely on the set of 20 canonical amino acids to perform their functions, additional chemical groups are required for some of the biological activities. These groups are brought by rare amino acids such as selenocysteine or pyrrolysine, by post-translational modifications or by cofactors. Considerable work has been made for expanding the genetic code in order to direct the incorporation of non-standard amino acids at desired positions in polypeptides. Two types of approaches were used, using either living cells or *in vitro* reconstituted ribosomal translation systems.

A key requirement for *in vivo* approaches is to ensure the availability of tRNA aminoacylated with the non-standard amino acid. In some cases, this has been done using mutated aminoacyl-tRNA synthetases (aaRS) able to aminoacylate a wild-type tRNA. For instance, *E. coli* methionyl-tRNA synthetase mutants were selected for aminoacylation of $tRNA^{Met}$ with the methionine surrogate azidonorleucine, resulting in efficient protein labelling *in vivo* in either bacterial or eukaryotic cells (Mahdavi et al., 2016; Ngo et al., 2009; Tanrikulu et al., 2009). The early studies led to the development of more general residue-specific methods that allow partial to quantitative replacement of canonical amino acids by non-canonical analogues (Johnson et al., 2010). For site-specific incorporation, the non-standard amino acid is generally encoded by a non-sense or a frameshift codon (Chin, 2017; Liu and Schultz, 2010). In this case, an orthogonal tRNA, not recognized by any endogeneous aaRS, is used together with an orthogonal aaRS, unable to aminoacylate any endogeneous tRNA (Wang et al., 2006). *In vitro* approaches generally use cell-free systems reconstituted from purified components (Shimizu et al., 2001). One important advantage of such systems is that aminoacyl-tRNAs can if necessary be prepared using methods that do not require aminoacylation by aaRSs. Indeed, highly flexible methods for *in vitro* aminoacylation of tRNAs with a wide variety of amino acids are available. These methods are based on RNA catalysts named flexizymes (Murakami et al., 2003, 2006; Ohuchi et al., 2007) and have virtually no limitation of acid donor substrates.

Most non-standard amino acids successfully used for *in vivo* incorporation were L-α-amino acids, resulting in the same polypeptide backbone as the canonical amino acids. β-amino acids bear an additional methylene group either between the nitrogen atom and the α-carbon ($\beta^2$ type) or between the α-carbon and the carboxylate carbon

* Corresponding authors.
*E-mail addresses:* emmanuelle.schmitt@polytechnique.edu (E. Schmitt), yves.mechulam@polytechnique.edu (Y. Mechulam).

https://doi.org/10.1016/j.jsb.2019.107435
Received 4 September 2019; Received in revised form 15 November 2019; Accepted 13 December 2019
Available online 17 December 2019

($\beta^3$ type) that results, when incorporated in a polypeptide, in a non-standard main chain. These non-canonical amino acids have deserved increasing interest because they give polypeptides unique properties, such as increased resistance to enzymatic hydrolysis (Heck et al., 2006; Webb et al., 2005) or the capacity to form peculiar helical structures (Petersson et al., 2007; Petersson and Schepartz, 2008; Seebach et al., 2006). Actually, β-amino acids were used to create peptides with interesting biological activities (Cheloha et al., 2015; Seebach and Gardiner, 2008).

Ribosomes could be modified to allow incorporation of βamino acids in cell free systems (Dedkova et al., 2011; Maini et al., 2013). It was also shown that various β-amino acids were compatible with ribosomal translation (Fujino et al., 2016). Moreover, elongation of peptides with successive β-amino acids was more recently rendered possible thanks to the use of engineered tRNAs having enhanced affinities for elongation factors EF-Tu and EF-P (Katoh and Suga, 2018). These studies in cell-free systems required the supply of β-aminoacyl-tRNAs synthesized using flexizymes or chemical tools. Overall, the availability of aaRSs able to specifically aminoacylate tRNAs with $\beta^3$-amino acids remains a bottleneck for their incorporation into polypeptides *in vivo*. Indeed, only few studies are available. For instance, mass spectrometry-based approaches have demonstrated the potential of aaRSs to use a wide variety of non-natural amino acids, including β-amino acids (Hartman et al., 2007, 2006). More recently, the capacity of some aaRS to use $\beta^3$-amino acids was studied kinetically and $\beta^3$-Phe analogues were successfully incorporated into dihydrofolate reductase in *E. coli* (Melo Czekster et al., 2016).

Here, we report a detailed study of the recognition of $\beta^3$-Met by *E. coli* methionyl-tRNA synthetase (MetRS). In particular, we show that the interpretation of kinetic studies can be obscured by the presence of contaminating α-Met in commercial $\beta^3$-Met samples and that the enzyme has limited capacities to activate $\beta^3$-Met. However, MetRS binds $\beta^3$-Met rather efficiently. We also describe a high-resolution crystallographic structure of the MetRS: $\beta^3$-Met complex that allows understanding why $\beta^3$-Met activation is poorly efficient. This structure will serve as a basis for engineering MetRS with improved $\beta^3$-Met aminoacylation capabilities.

## 2. Results and discussion

### 2.1. Evidence for the presence of contaminating α-Met in $\beta^3$-Met samples

It is well established that interpretation of [$^{32}$P]ATP-PPi exchange experiments can be obscured by the presence of methionine traces in commercial amino acids samples (Fersht and Dingwall, 1979). Prior to studying activation of $\beta^3$-Met by MetRS, we used LC-HRMS experiments to search for the presence of α-Met in the $\beta^3$-Met sample. A protonated molecule at *m/z* 164.074 (corresponding to $\beta^3$-MetH$^+$; retention time of 2.4 min) was mainly observed on the ESI-P mass spectrum for the $\beta^3$-Met sample (Fig. 1). However, the results showed the presence of a compound having the exact molecular mass of α-MetH$^+$ (*m/z* 150.058) at 2.2 min in $\beta^3$-Met suggesting the occurrence of contaminating α-Met. Accordingly, the peak of contaminating α-Met corresponded to the major peak observed in an α-Met sample analyzed as a reference (data not shown). From the relative responses of the $\beta^3$-Met and α-Met samples, we evaluated the contamination of α-Met in the $\beta^3$-Met sample of about 0.1%. Actually, BOC-L-methionine was used as a reactant during the synthesis of $\beta^3$-Met, as communicated by the company from which the compound was purchased. As an attempt to remove contamination, we treated $\beta^3$-Met samples with methionine gamma lyase (MGL), an enzyme that degrades L-methionine into methanethiol, ammonia and 2-oxobutanate. This enzyme was likely to be specific of α-Met as compared to $\beta^3$-Met since it binds both the amino and carboxylate groups of methionine (Fukumoto et al., 2014). The treated sample was then analyzed by mass spectrometry (Fig. 1). As expected, the molecular ion at *m/z* 150.058 [α-MetH]$^+$ became undetectable in the MGL sample (reduced by a factor of at least ten), whereas the peak corresponding to $\beta^3$-Met remained present.

### 2.2. MetRS binds $\beta^3$-Met

Because of this contamination, we investigated binding of $\beta^3$-Met using enzyme intrinsic fluorescence titration experiments. This method is much less sensitive than ATP-PPi exchange to trace contaminations. Indeed, enzyme fluorescence varies measurably only if a significant proportion of the enzyme is bound to the ligand whereas even a very small fraction of enzyme bound to α-Met can catalytically give detectable accumulation of the [$^{32}$P]PPi reaction product. It is known that MetRS displays large variations of intrinsic fluorescence when binding methionine or methionyl adenylate from which useful thermodynamic parameters can be derived. Throughout this study, we used a His-tagged M547 monomeric version of *E. coli* MetRS, fully active, both *in vitro* and *in vivo* (Schmitt et al., 2009). Addition of $\beta^3$-Met to MetRS caused an increase of intrinsic tryptophan fluorescence, similar to the increase caused by titration with α-Met. A dissociation constant of 1.2 ± 0.2 mM for the MetRS: $\beta^3$-Met complex was derived from the titration data (Fig. 2 and Table 1). This value was only 24-fold higher than the Kd of MetRS: α-Met. According to the 0.1% contamination level of α-Met in our $\beta^3$-Met sample, the concentration of α-Met in the titration experiments did not exceed 4 μM. Because this value was low as compared to the Kd of α-Met for MetRS (50 μM, Table 1), we concluded that the contaminating α-Met could not influence the measured Kd value of $\beta^3$-Met. Consistent with this conclusion, no detectable effect on the dissociation constant of the MetRS: $\beta^3$-Met complex was observed if $\beta^3$-Met was treated with MGL prior to the measurement (Fig. 2). This latter result also showed that the non-canonical amino acid was not affected by MGL treatment.

### 2.3. Interpretation of the [$^{32}$P]ATP-PPi exchange assay is obscured by amino acid contamination

Measurement of the apparent catalytic parameters ($k_{cat\text{-}app}$ and $K_{m\text{-}app}$ for $\beta^3$-Met) of the [$^{32}$P]ATP-PPi isotopic exchange reaction using the commercial $\beta^3$-Met sample showed that as compared to α-Met, $k_{cat\text{-}app}$ was lowered by a factor of 42 (1.2 $s^{-1}$ as compared to 50 $s^{-1}$) whereas $K_{m\text{-}app}$ was increased by a factor of 35 (630 μM as compared to 18 μM). Overall, the catalytic efficiency of the isotopic exchange reaction was reduced by an apparent factor of *ca* 1500 when α-Met was replaced by $\beta^3$-Met. Notably, these results were at odd with those of a study reporting that MetRS was very tolerant to the substitution of α-Met by $\beta^3$-Met, with only a modest (2-fold) preference for Met in ATP-PPi exchange (Melo Czekster et al., 2016). Moreover, in the presence of 2 mM $\beta^3$-Met treated with MGL, the isotopic exchange rate dropped to 0.07 $s^{-1}$ as compared to 0.9 $s^{-1}$ in the presence of 2 mM untreated $\beta^3$-Met (a value in agreement with $k_{cat\text{-}app}$ of 1.2 $s^{-1}$ and $K_{m\text{-}app}$ of 0.63 mM). This result showed that, at least with the commercial sample, the $\beta^3$-Met-dependent [$^{32}$P]ATP-PPi exchange rate mostly reflected activation of contaminating α-Met. The exchange rates measured when varying the concentration of untreated $\beta^3$-Met were therefore interpreted using a competitive inhibition scheme (Fig. 3). In this scheme, $\beta^3$-Met binds the enzyme at a site overlapping the α-Met site but cannot be activated. Fitting showed that the experimental results were consistent with activation of $\beta^3$-Met occurring at a negligible rate and $\beta^3$-Met being contaminated with 0.09% α-Met (mol/mol; Fig. 3). Notably, this level of contamination was compatible with the results of mass spectrometry analyses of $\beta^3$-Met. Finally, traces of α–Met were also evidenced in enzyme preparations. Attempts to diminish the contamination to a level where $\beta^3$-Met-dependent [$^{32}$P]ATP-PPi exchange rates can be accurately measured were unsuccessful. Because of the high sensitivity of ATP-PPi isotopic exchange to the presence of traces of α-Met, we concluded that this method was not suitable to detect a possible activation of $\beta^3$-Met by MetRS.

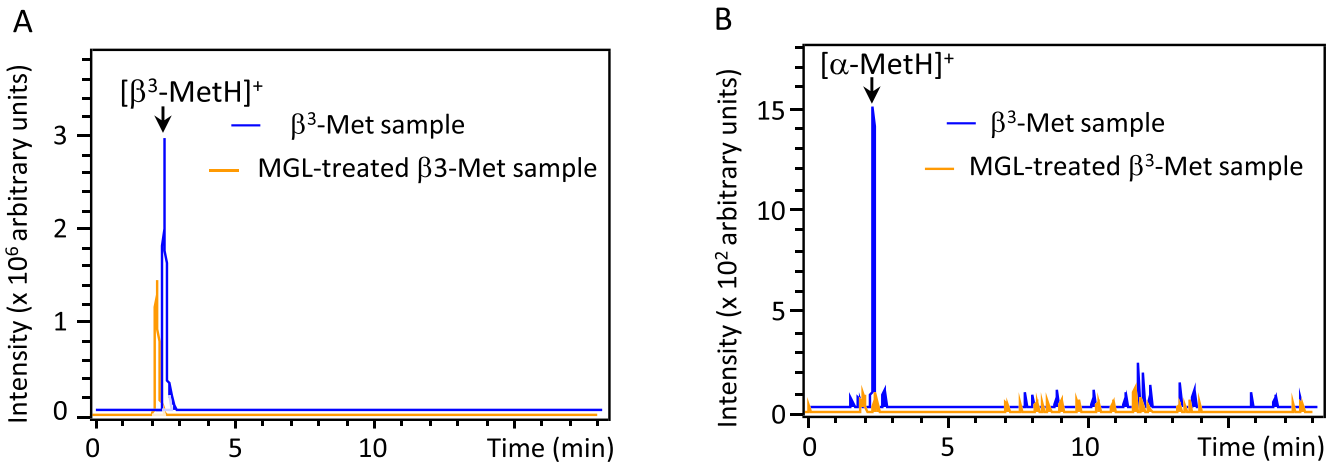


**Fig. 1.** LC-HRMS analysis of $\beta^3$-Met (blue) and MGL-treated $\beta^3$-Met (yellow) samples. Extracted ion current (EIC) chromatograms of (A) *m/z* 164.074 ± 0.001 corresponding to $[\beta^3\text{-MetH}]^+$ ($C_6H_{14}NO_2S$) and (B) *m/z* 150.058 ± 0.001 corresponding to $[\alpha\text{-MetH}]^+$ ($C_5H_{12}NO_2S$). The blue chromatograms were shifted to the right for clarity. (For interpretation of the references to colour in this figure legend, the reader is referred to the web version of this article.)

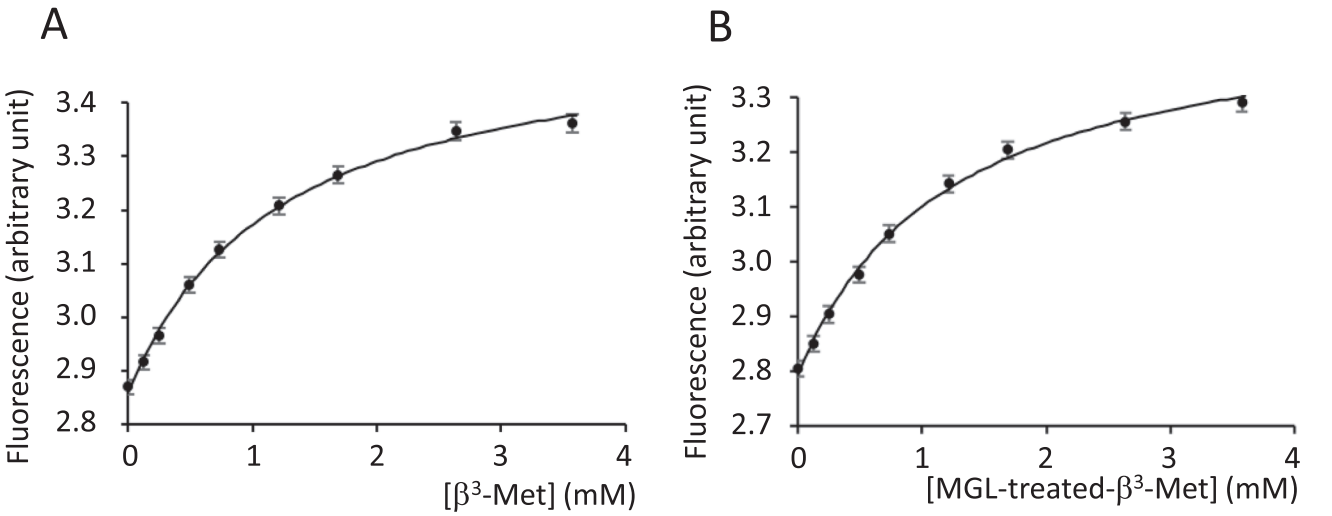


**Fig. 2.** Intrinsic enzyme fluorescence titration of MetRS with $\beta^3$-Met. Panel A: MetRS (0.5 μM) was titrated with increasing amounts of commercial $\beta^3$-Met, as described in Materials and Methods. The experimental points show the measured fluorescence as a function of the concentration of $\beta^3$-Met. Data were fitted to a simple equilibrium model using standard least-square procedures. The curve shows the resulting fit (Kd = 1.2 mM). Panel B: Same experiment but $\beta^3$-Met was treated with MGL before titration (Kd = 1.2 mM).

**Table 1**
Kinetic and thermodynamic constants of α-Met or $\beta^3$-Met binding, activation and aminoacylation by wild-type MetRS and the VI298 variant. Dissociation and rate constants are defined in Scheme 1. Each experiment was performed at least twice independently. Results are expressed as mean ± either standard deviation from the independent experiments or standard error from the fitting procedure, whichever the greater.

| Enzyme/Substrate | WT/α-Met | WT/$\beta^3$-Met | V298I/α-Met | V298I/$\beta^3$-Met |
|---|---|---|---|---|
| $K_{Met}$ (mM) | 0.05 ± 0.01 | 1.2 ± 0.2 | 0.029 ± 0.001 | 0.56 ± 0.01 |
| $K_{Met}^{ATP}$(mM) | 0.070 ± 0.004 | 0.30 ± 0.04 | 0.063 ± 0.004 | 0.15 ± 0.02 |
| $k_f$ ($s^{-1}$) | 260 ± 10 | 0.051 ± 0.003 | 262 ± 12 | 0.057 ± 0.005 |
| $K_{PP}$ (mM) | 0.075 ± 0.025 | 1.0 ± 0.25 | 0.06 ± 0.01 | 0.8 ± 0.2 |
| $k_b$ ($s^{-1}$) | 189 ± 23 | 1.2 ± 0.3 | 195 ± 30 | 0.95 ± 0.2 |
| Aminoacylation rate ($s^{-1}$) | 0.52 ± 0.07 | (5.6 ± 0.3) $10^{-4}$ | n.d. | n.d. |

Aminoacylation rates were measured in the presence of 2 μM tRNA, 2 mM ATP and 2 mM of either α-Met or $\beta^3$-Met. Results are the mean ± sd from two independent experiments.

### *2.4. $\beta^3$-Met is a poor substrate of MetRS*

As described above, fluorescence titration can be used to follow the bindings of α-Met or $\beta^3$-Met to MetRS. It is also known that addition of ATP in the presence of magnesium ions to the MetRS:Met complex leads to a large decrease of fluorescence intensity reflecting synthesis of methionyl adenylate. Hence, a MetRS: $\beta^3$-Met complex formed in the presence of MGL-treated $\beta^3$-Met was mixed with ATP-$Mg^{2+}$. We observed a slow increase in fluorescence (rate constant of the order of 0.05 $s^{-1}$), contrasting with the fast decrease observed in the case of α-Met adenylate formation. However, importantly, this increase in fluorescence was reversed by the subsequent addition of

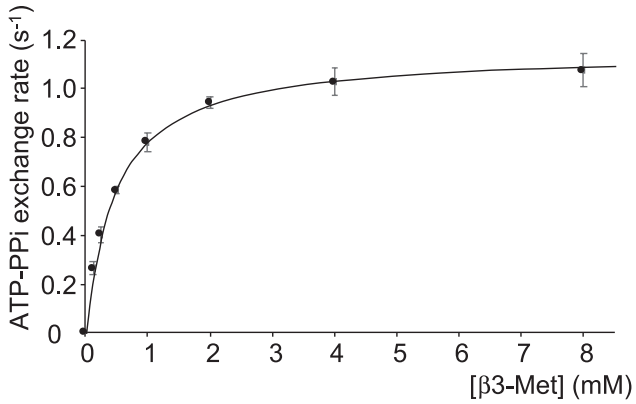


**Fig. 3.** Fitting the $\beta^3$-Met-dependent [$^{32}$P]ATP-PPi exchange with a competition model. Initial rates of [$^{32}$P]ATP-PPi exchange catalyzed by MetRS were measured in the presence of 2 mM ATP and various concentrations of commercial $\beta^3$-Met. Data (average from three independent experiments) were fitted to a classical competitive inhibition scheme, where isotopic exchange depends on contaminating α-Met. Adjusted parameters for fitting were the contamination rate λ ([α-Met]/[$\beta^3$-Met]) and the inhibition constant $K_I$. The curve shows the best fit to the experimental data, with a contamination rate of $(8.9 \pm 0.3)\cdot10^{-4}$ and an inhibition constant of 477 ± 21 μM. Michaelian parameters of the α-Met-dependent exchange were measured with the same batch of enzyme ($k_{cat}$ = 50 $s^{-1}$ and $K_m$ = 18 μM) and kept constant in the fitting procedure. The theoretical equation giving the initial rate (vi) as a function of the concentration of $\beta^3$-Met ([S]) was: $vi = k_{cat}\,[E]\frac{[S]}{[S]+\frac{Km}{\lambda}\left(1+\frac{[S]}{K_I}\right)}$.

pyrophosphate, suggesting that it could be due to the formation of $\beta^3$-Met adenylate. In order to unambiguously confirm the formation of $\beta^3$-Met adenylate, we analyzed the product of the reaction of ATP-$Mg^{2+}$ with MetRS: $\beta^3$-Met using LC-HRMS (Fig. 4A). These experiments clearly identified an ion at *m/z* 493.127 with elemental composition of $C_{16}H_{26}N_6O_8PS$ corresponding to protonated $\beta^3$-Met adenylate. This product was not present in the control sample where the reaction was stopped immediately after addition of MetRS (Fig. 4A). As expected, the corresponding ion for α-Met (*m/z* 479) was not observed. To obtain structural characterization of this compound, LC-HRMS/MS experiments have been carried out on the molecular ion (Fig. 4B). Three major ions were obtained. The ion at *m/z* 348.07 was formed from *m/z* 493.127 by elimination of $C_6H_{15}NO$ according with its elemental composition $C_{10}H_{15}N_5O_7P$ and corresponded to protonated AMP. Ions at *m/z* 164.074 ($C_{10}H_{15}N_5O_7P$) and *m/z* 136.062 ($C_5H_6N_5$) were formed from the molecular ion and correspond to the protonated $\beta^3$-Met and adenine, respectively. A fragmentation mechanism of the *m/z* 493 ion is proposed in the Supplementary Scheme S1. These results clearly confirmed the identification of the reaction product as $\beta^3$-Met adenylate.

The experiments described above showed that the increase in intrinsic enzyme fluorescence observed during reaction of MetRS with MGL-treated $\beta^3$-Met and ATP-$Mg^{2+}$ indeed reflected the synthesis of $\beta^3$-methionyl adenylate. We therefore measured the rates of fluorescence variation in the presence of 2 mM ATP-$Mg^{2+}$ and increasing amounts of MGL-treated $\beta^3$-Met in order to derive the thermodynamic constants of the reaction, K $\beta^3_{\text{-Met}}{}^{\text{ATP}}$, the dissociation constant of $\beta^3$-Met from the MetRS:ATP-$Mg^{2+}$ complex and $k_f$ β, the rate of $\beta^3$-methionyl adenylate synthesis (Scheme 1, Supplementary Fig. S1). The results (Table 1) showed that affinity of $\beta^3$-Met for the MetRS:ATP-$Mg^{2+}$ complex was reduced by one order of magnitude as compared to that of α-Met, and that the rate of activation of the β amino acid was 5200-fold lower than that of canonical methionine. Similarly, the enzyme remained able to catalyze the reversion of enzyme-bound $\beta^3$-methionyl adenylate by PPi-$Mg^{2+}$, though at a rate reduced by a factor of 157 as compared to the reversion of α-methionyl adenylate. Overall, these experiments showed that MetRS was indeed able to activate $\beta^3$-Met, but with a catalytic efficiency ($k_f$ β/K $\beta^3_{\text{-Met}}{}^{\text{ATP}}$) reduced by four orders of magnitude as compared to canonical methionine. This low catalytic efficiency was mainly caused by small $k_f$ β and $k_b$ β kinetic constants, reflecting a non-optimal stabilization of the transition state of the activation reaction according to the Arrhenius law.

Finally, we examined the ability of MetRS to transfer $\beta^3$-Met onto $tRNA_f^{Met}$. This was first done by analyzing the products of aminoacylation reactions (see methods) using mass spectrometry after digestion with S1 nuclease (Hartman et al., 2007, 2006). The results showed the presence of a product corresponding to AMP esterified with $\beta^3$-methionyl-AMP (molecular ion at *m/z* 493.127) whereas no α-methionyl-AMP was detected (Fig. 4C). In order to prevent deacylation during sample preparation and to have a better signal in MS/MS, an aliquot of the aminoacyl-tRNA was N-acetylated using acetic anhydride prior to S1 nuclease digestion. Consistent with our expectations, N-acetyl-$\beta^3$-methionyl-AMP ($MH^+$ *m/z* 535.138) was found in the acetylated sample whereas N-acetyl-α-methionyl-AMP ($MH^+$ *m/z* 521.121) was absent (Fig. 4C). Reference experiments with α-Met instead of $\beta^3$-Met gave the expected results (Fig. 4D). Identifications of N-acetyl-$\beta^3$-methionyl-AMP and N-acetyl-α-methionyl-AMP were further confirmed using HR-MS/MS of protonated compounds. Supplementary Table S1 brings together the detected fragments ions for both compounds. These results allowed us to propose the fragmentation scheme of protonated molecules reported in Supplementary Scheme 2.

We finally measured the rate of tRNA aminoacylation with $\beta^3$-Met using the assay based on [3′-$^{32}$P]-labelled tRNA (Ledoux and Uhlenbeck, 2008). In the presence of 2 mM MGL-treated $\beta^3$-Met and 2 mM ATP, MetRS catalyzed the aminoacylation of $tRNA_f^{Met}$ (2 μM) at a rate three orders of magnitude lower than the rate measured in the control experiment with α-Met (Fig. 5 and Table 1). It should be underlined that the rate value measured with $\beta^3$-Met must be taken cautiously since, even after treatment with MGL, traces of α-Met remain. Nevertheless, taking into account the mass spectrometry experiments, the results show that MetRS can transfer $\beta^3$-Met onto tRNA though at a reduced rate, in agreement with the reduced efficiency of the $\beta^3$-Met activation step as compared to the Met activation step.

### 2.5. Structural study of $\beta^3$-Met binding to MetRS

The results described above raise the question of how $\beta^3$-Met is recognized by MetRS. Understanding this may also guide efforts aimed at engineering the enzyme for more efficiency and specificity towards the β amino acid. We therefore crystallized the enzyme in the presence of $\beta^3$-Met. This was done by microseeding a supersaturated (1.08 M ammonium citrate, 6 °C) enzyme solution containing 20 mM $\beta^3$-Met with crystals of the unliganded enzyme. Using such crystals, a complete dataset was obtained at 1.45 Å resolution (Table 2). For better comparison of α-Met and $\beta^3$-Met binding sites, we also grew crystals of the MetRS: α-Met complex and obtained an X-ray diffraction dataset at 1.2 Å resolution. The previously published structure of the MetRS: α-Met complex was indeed determined at a lower 1.85 Å resolution (PDB id 1F4L, (Serre et al., 2001)). To avoid any bias, the two structures were solved by molecular replacement using the structure of unliganded MetRS as a search model (PDB id 1QQT, (Mechulam et al., 1999a). In both cases, the presence of the ligand was obvious in the molecular replacement density map. The structures were then refined using successive rounds of manual rebuilding in Coot and energy minimization in Phenix. Final R/Free-R values were 0.092/0.126 (MetRS: $\beta^3$-Met) complex and 0.145/0.171 (MetRS: α-Met complex; Table 2). The enzyme is made up of an N-terminal Rossmann fold containing the catalytic centre (Mechulam et al., 1991; Schmitt et al., 1994) and a C-terminal helix-bundle domain responsible for recognition of the CAU anticodon of $tRNAs^{Met}$.

As previously described (Crepin et al., 2003; Serre et al., 2001; Tanrikulu et al., 2009), binding of α-Met caused a dramatic rearrangement of aromatic residues. The side chains of W229, W253, F300 and F304 rotate such that W229 stacks on F304 and W253 stacks on F300. Furthermore, Y15 rotates, acting as a lid that locks the amino

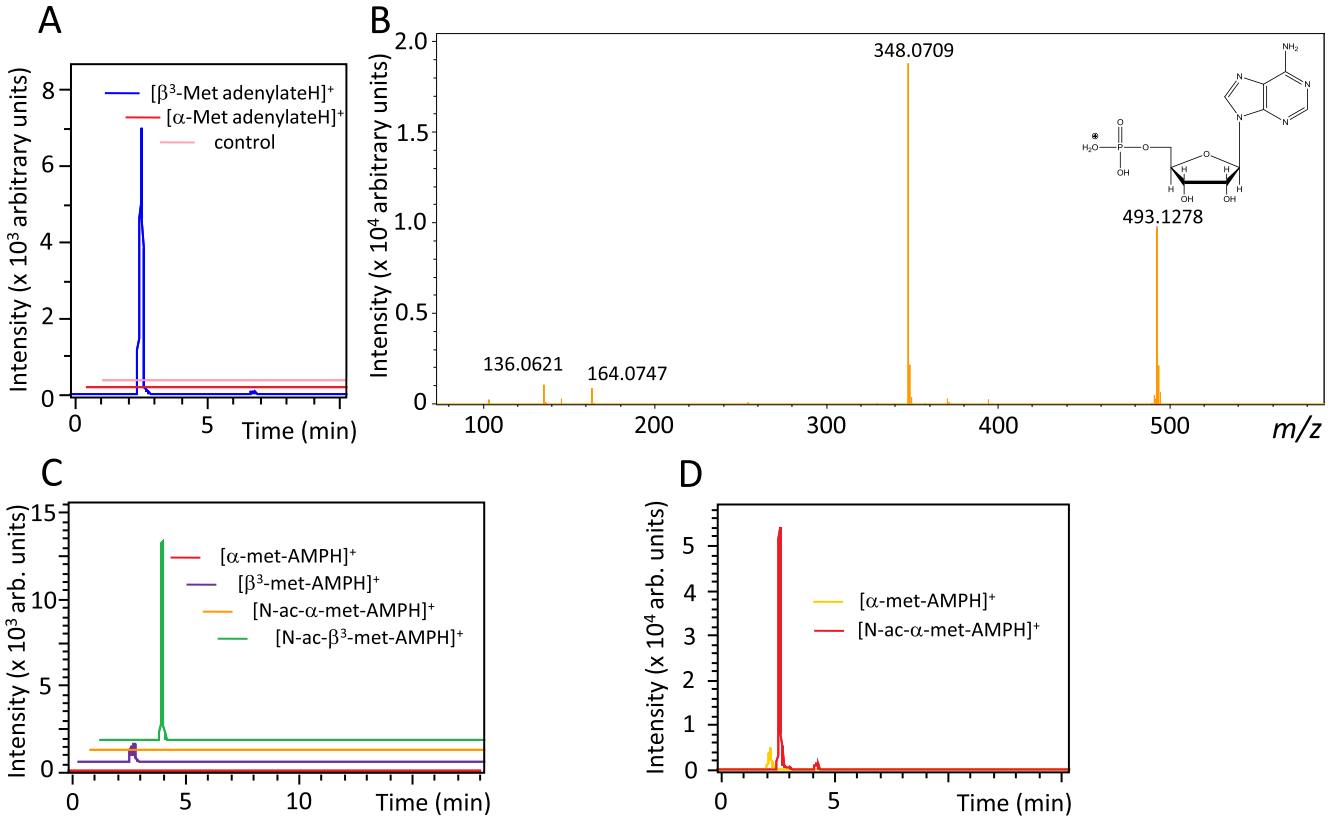


**Fig. 4.** LC-HRMS analyses of MGL-treated β$^3$-Met activation and transfer onto tRNA$_f^{Met}$. Panel A: Analysis of the products of the activation reaction. The red and blue chromatograms in correspond to the sample in which MetRS was reacted with ATP and MGL-treated β$^3$-Met. Extracted ion current (EIC) chromatograms of *m/z* 479.111 ± 0.001 (red, corresponding to [α-Met adenylateH]$^+$ $C_{15}H_{24}N_6O_8PS$) and of *m/z* 493.126 ± 0.001 (blue, corresponding to [β$^3$-Met adenylateH]$^+$ $C_{16}H_{26}N_6O_8PS$). The pink chromatogram corresponds to *m/z* 493.126 ± 0.001 ([β$^3$-Met adenylateH]$^+$) for the zero reaction time control sample. Panel B:HR-MS/MS ($E_{col}$ = 15 eV) of the *m/z* 493.1263 ion obtained at 2.6 min retention time (blue chromatogram in Panel A). The proposed mechanism for the decomposition of the molecular ion is indicated on the Supplementary Scheme 1. Panel C:LC-HRMS analysis of the aminoacylation reaction in the presence of MGL-treated β$^3$-Met. The samples were submitted to S1 nuclease cleavage as indicated in Materials and Methods. The panel shows the extracted ion current chromatograms (EIC) of *m/z* 479.111 ± 0.001 (corresponding to [α-methionyl-AMPH]$^+$, $C_{15}H_{24}N_6O_8PS$; red) and *m/z* 493.126 ± 0.001 (corresponding to [β$^3$-methionyl-AMPH]$^+$, $C_{16}H_{26}N_6O_8PS$; purple). The two other chromatograms correspond to the samples acetylated prior to S1 cleavage, showing the EIC of *m/z* 521.121 ± 0.001 (corresponding to [N-acetyl-α-methionyl-AMPH]$^+$, $C_{17}H_{26}N_6O_9PS$; orange) and *m/z* 535.138 (corresponding to [N-acetyl-β$^3$-methionyl-AMPH]$^+$, $C_{18}H_{28}N_6O_9PS$; green). The panel shows the presence of the compounds expected from the transfer of β$^3$-Met onto tRNA and the absence of detectable aminoacylation with α-Met. Panel D: Reference aminoacylation experiment using α-Met instead of β$^3$-Met, with (red) or without (yellow) acetylation. The panel shows the EIC of *m/z* 479.111 ± 0.001 (corresponding to [α-methionyl-AMPH]$^+$, $C_{15}H_{24}N_6O_8PS$; yellow) and *m/z* 521.121 ± 0.001 (corresponding to [N-acetyl-α-methionyl-AMPH]$^+$, $C_{17}H_{26}N_6O_9PS$ ; red). The ions at *m/z* 535.138 ([N-acetyl-β$^3$-methionyl-AMPH]$^+$) and *m/z* 521.121 ([N-acetyl-α-methionyl-AMPH]$^+$) were further characterized by HR-MS/MS (Supplementary Table 1 and Supplementary Scheme 2). (For interpretation of the references to colour in this figure legend, the reader is referred to the web version of this article.)

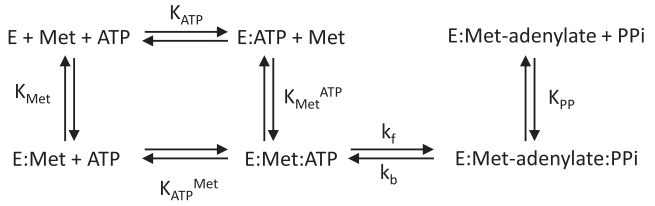


**Scheme 1.** Scheme for methionyl adenylate synthesis and reversion by MetRS. The scheme defines the five dissociation constants and the two rate constants $k_f$ and $k_b$.

acid in its binding cavity (Fig. 6). These induced rearrangements reduce the size of the cavity and allow accommodation of the methionine side-chain. The α-Met cavity is bordered by L13, W253, P257, Y260 and I297. The amino group of the substrate is held by the side chain of D52 and by the main chain carbonyl of L13. The carboxylate is adequately positioned for reacting with the α-phosphoryl group of ATP, as suggested from comparison with MetRS structures bound to methionyl adenylate or analogues (Fig. 6, Crepin et al., 2003; Larson et al., 2011). Such a precise positioning of the carboxylate group with respect to ATP was also observed in class 2 aminoacyl-tRNA synthetases (Schmitt et al., 1998).

Comparison of the MetRS: β$^3$-Met structure with the MetRS: α-Met one showed very high similarity. The side chain of β$^3$-Met was bound in the same induced pocket as that of α-Met, without any significant positional difference (Fig. 6 and Supplementary Fig. S2). In particular, the rearrangement of aromatic residues (W229, W253, F300 and F304) occurred identically. Also, the amino group was located at the same position as that of α-Met, bound to D52 and L13. However, because of the insertion of a methylene group, the carboxylate of β$^3$-Met is positioned differently as compared to α-Met (Fig. 6). More precisely, two alternative positions differing by a rotation of about 87° around the C α-C β bond were observed for the carboxylate of β$^3$-Met (Fig. 6 and Fig. S2). In the major conformation (70% occupancy), the carboxylate oxygens were oriented away from the active site. In this conformation, Y15 cannot reach the position where it locks the active site. Accordingly, Y15 was observed at several alternative positions, ranging from the open position seen in the unliganded enzyme to the closed position seen in the MetRS: α-Met complex (Fig. 6 and Fig. S2). In contrast, in

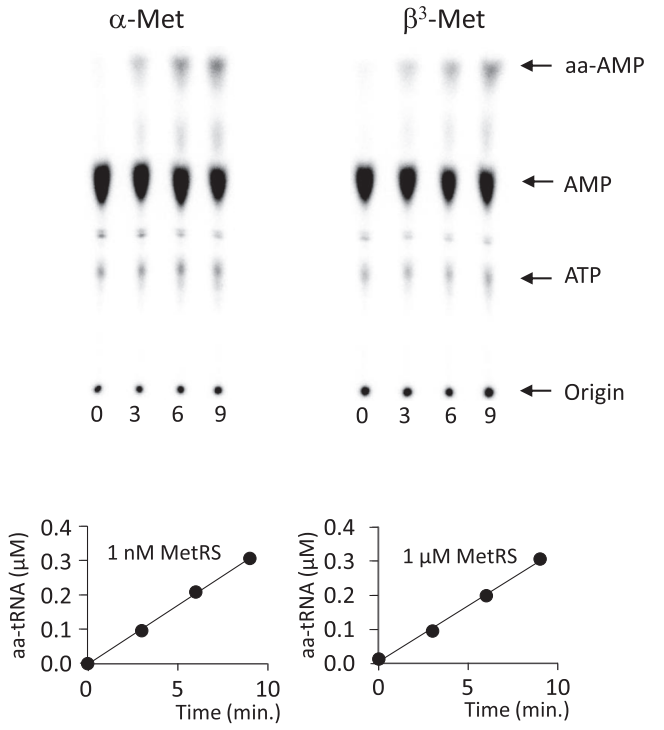


**Fig. 5.** Aminoacylation of $tRNA_f^{Met}$ by MGL-treated $\beta^3$-Met. [3′-$^{32}$P]-labelled $tRNA_f^{Met}$ was aminoacylated with α-Met in the presence of 1 nM MetRS or with MGL-treated $\beta^3$-Met in the presence of 1 μM MetRS (see Materials and Methods). At the indicated times, aliquots were withdrawn and digested with S1 nuclease. The resulting digests were analyzed by TLC. The figure shows the results of a typical experiment with the fluorogram in the upper part and the corresponding image analysis in the bottom part. The figure shows that the rates differ by three orders of magnitude. The average rates from two independent experiments are reported in Table 1.

the minor conformation, one carboxylate oxygen of $\beta^3$-Met is located only at 1.3 Å from the ideal position observed in α-Met and full rotation of Y15 is possible.

With α-Met, the electrostatic hindrance between the carboxylate group and the α-phosphoryl of ATP is known to be compensated by strong synergistic binding such that K $\alpha_{\text{-Met}}$ and K $\alpha_{\text{-Met}}^{ATP}$ have similar values (Table 1; Blanquet et al., 1975; Fayat et al., 1977). With $\beta^3$-Met, the affinity of the amino acid was 4-fold higher in the presence of ATP, showing that the electrostatic repulsion was less intense. This agrees with the structural observation that the carboxylate of $\beta^3$-Met is not adequately positioned to react with the α-phosphoryl of ATP.

Furthermore, in the $\beta^3$-Met complex, the D296-Y325 couple has two alternative conformations. In the first conformation (hereafter termed "OUT"), the Y325 hydroxyl group formed a hydrogen bond with the side chain of D296. In the other conformation (hereafter termed "IN"), Y325 was shifted, causing a rotation of D296 towards the active site. The "OUT" conformation is found in the structures of unliganded MetRS and of the MetRS: α-Met complex, whereas the "IN" conformation is found in the structures of MetRS:methionyl adenylate analogues complexes (Crepin et al., 2003; Mechulam et al., 1999b; Schmitt et al., 2009; Serre et al., 2001). Notably, D296 is conserved in class 1 aaRS and plays an important role in the catalysis of aminoacyl adenylate synthesis (Brick et al., 1989; Crepin et al., 2003; Fersht, 1987). These constraints on D296 may therefore contribute to a reduced efficiency for $\beta^3$-Met activation.

Overall, the structural results illustrate how the formation of aminoacyl adenylate from $\beta^3$-Met and ATP can occur, though at a reduced rate, as observed in the kinetic measurements (Table 1).

### 2.6. Attempt to enhance activity of MetRS towards $\beta^3$-Met

Interestingly, on the side of the amino acid-binding pocket opposite to the active centre, a supplementary $\beta^3$-Met minor site with an occupancy of 0.7 was observed. The second $\beta^3$-Met molecule (hereafter termed $\beta^3$-$Met_2$) was bound between loop 295–297 connecting β D to αD on the one hand and helix α4 in the connective polypeptide (CP) on the other hand (Fig. 7). The secondary binding cavity is bordered by V214, K217, W221, K295, V298 and Y325. As described above, Y325 is connected to D296, thereby showing a physical link between the active site and the secondary $\beta^3$-Met site. We therefore wondered whether occupation of the $\beta^3$-$Met_2$ site may affect the activity of MetRS towards $\beta^3$-Met. In order to impair $\beta^3$-$Met_2$ binding, we mutated V298 into I. Measurement of the catalytic parameters of $\beta^3$-Met activation showed a two-fold increase in affinity of $\beta^3$-Met for the V298I mutant, both in the presence and in the absence of ATP (Table 1). This effect was however paralleled by a two-fold increase in α-Met affinity, at least in the absence of ATP. Therefore, selectivity of the V298I mutant towards $\beta^3$-Met as compared to α-Met was not enhanced by a factor greater than 2.

The structure of the V298I mutant was solved in the apo form and bound to either α-Met or $\beta^3$-Met (Fig. 7B,C,D). As expected, the β amino acid was found only in the main site. However, in the V298I: $\beta^3$-Met structure, D296 was still observed in the "IN" and "OUT" conformations. Moreover, both conformations of D296 were also observed in the apo and α-Met-bound forms of the V298I mutant. Hence, occupation of the $\beta^3$-$Met_2$ cavity by the Ile side-chain was unfortunately sufficient to cause destabilization of the D296 position, meaning that the mutation did not have the desired structural effect. However, in the apo form, alternative conformations for W229 and W253, two residues involved in the conformational rearrangement of aromatic residues induced by α-Met or $\beta^3$-Met binding were observed (Supplementary Fig. S3). Therefore, the enhanced affinity of the V298I mutant for both $\beta^3$-Met and α-Met may have been caused by a better propensity to adopt a conformation corresponding to the conformation induced by Met binding.

### 2.7. Concluding remarks

This study shows that *E. coli* MetRS is able to use $\beta^3$-Met as a substrate in both the amino acid activation and $tRNA_f^{Met}$ aminoacylation reactions. These results are in keeping with previous studies showing that several β amino acids, including $\beta^3$-Met, could be transferred onto tRNA by the corresponding aminoacyl-tRNA synthetase (Hartman et al., 2007, 2006). The efficiency of the reaction appears however very low as compared to what was observed in a recent study (Melo Czekster et al., 2016). This discrepancy might be due to the presence of contaminating α-Met in commercial $\beta^3$-Met samples. The high-resolution structure of the MetRS: $\beta^3$-Met complex explains why the non-canonical amino acid has a rather good affinity for the enzyme but is activated *ca* 5000-fold more slowly. This is due to a non-optimal positioning of the carboxylate moiety, rendering reaction with the α-phosphoryl group of ATP difficult. $\beta^3$-Met can also bind in a secondary site, though less efficiently as suggested by partial occupancy in the structure in spite of the high concentration of amino acid used for crystallization (20 mM). Disrupting the secondary site had little, if any, influence on the efficiency of MetRS towards $\beta^3$-Met. Nevertheless, this study provides structural and functional foundations for MetRS engineering to obtain a more active and specific enzyme towards $\beta^3$-Met. Such an enzyme would open the possibility of directing site-specific incorporation of $\beta^3$-Met *in vivo*.

## 3. Materials and methods

### 3.1. Site-directed mutagenesis and enzyme purification

The gene encoding M547 from pBSM547+ (Mellot et al., 1989;

**Table 2**
Data collection and refinement statistics.

| | MetRS: β³-Met | MetRS: α-Met | VI298 | VI298: β³-Met | VI298: α-Met |
|---|---|---|---|---|---|
| Data collection | | | | | |
| Space group | $P2_1$ | $P2_1$ | $P2_1$ | $P2_1$ | $P2_1$ |
| Cell dimensions | | | | | |
| a, b, c (Å) | 78.23,45.23,86.25 | 78.28,45.19,85.89 | 78.51,45.53,86.31 | 78.31,45.11,86.21 | 78.47,45.15,86.23 |
| α, β, γ (°) | 90,107.36,90 | 90,107.39,90 | 90,107.38,90 | 90,107.39,90 | 90,107,48,90 |
| Resolution (Å) | 1.45 | 1.2 | 1.5 | 1.48 | 1.38 |
| $R_{sym}$ (%)[a] | 3.8 (16.0)[b] | 10.5 (164) | 7.6 (96.4) | 11.7 (103) | 6.8 (114) |
| I/σ(I) | 20.9 (7.9) | 10.0 (1.1) | 11.2(1.2) | 9.2 (1.3) | 15.9 (1.4) |
| Completeness (%) | 98.4 (95.1) | 99.0 (94.8) | 99.2 (97.4) | 99.6 (98.3) | 99.1 (95.6) |
| Redundancy | 3.3 (3.1) | 6.4 (6.2) | 4.7 (4.6) | 6.8 (6.6) | 6.8 (6.4) |
| $CC_{1/2}$ (%)[c] | 99.9 (96.9) | 99.8 (32.6) | 99.8 (95.2) | 99.8 (59.7) | 99.9 (52.3) |
| Refinement | | | | | |
| Resolution (Å) | 41.7–1.45 | 33.1–1.2 | 38.9–1.5 | 48.6–1.48 | 48.5–1.38 |
| No reflections | 101,094 | 178,894 | 93,868 | 96,417 | 116,836 |
| $R_{work}/R_{free}$ | 0.093/0.126 (0.092/0.136) | 0.136/0.167 (0.328/0.354) | 0.134/0.176 (0.282/0.337) | 0.133/0.168 (0.319/0.353) | 0.127/0.162 (0.289/0.323) |
| No atoms | | | | | |
| Protein | 4696 | 5057 | 4692 | 4709 | 4638 |
| Water | 810 | 746 | 679 | 740 | 685 |
| Non-protein[e] | 50 | 41 | 40 | 75 | 60 |
| B-factors (Å²) | | | | | |
| Protein | 13.1 | 16.7 | 22.2 | 17.7 | 19.2 |
| Water Non-protein | 33.2 | 35.6 | 39.5 | 35.8 | 36.1 |
| | 22.2 | 34.7 | 48.2 | 37.4 | 41.4 |
| r.m.s. deviations | | | | | |
| Bond lenghts (Å) | 0.011 | 0.008 | 0.008 | 0.008 | 0.008 |
| Bond angles (°) | 1.304 | 0.949 | 0.994 | 0.947 | 0.940 |

A single crystal was used for data collection.

[a] $R_{sym}$ (I) $= \frac{\sum_{hkl} \sum_i | \langle I_{hkl} \rangle - I_{hkl,i} |}{\sum_{hkl} \sum_i | I_{hkl} |}$, where i is the number of reflections hkl.

[b] Values in parentheses are for highest-resolution shell.

[c] CC(1/2) is the correlation coefficient between two random half data sets (Karplus and Diederichs, 2012).

[d] $R_{work} = \frac{\sum || F_{obs}| - |F_{calc} ||}{\sum | F_{obs}|}$; $R_{free}$ is calculated with 5% of the reflections.

[e] ligands and solvent molecules other than water (citrate and glycerol).

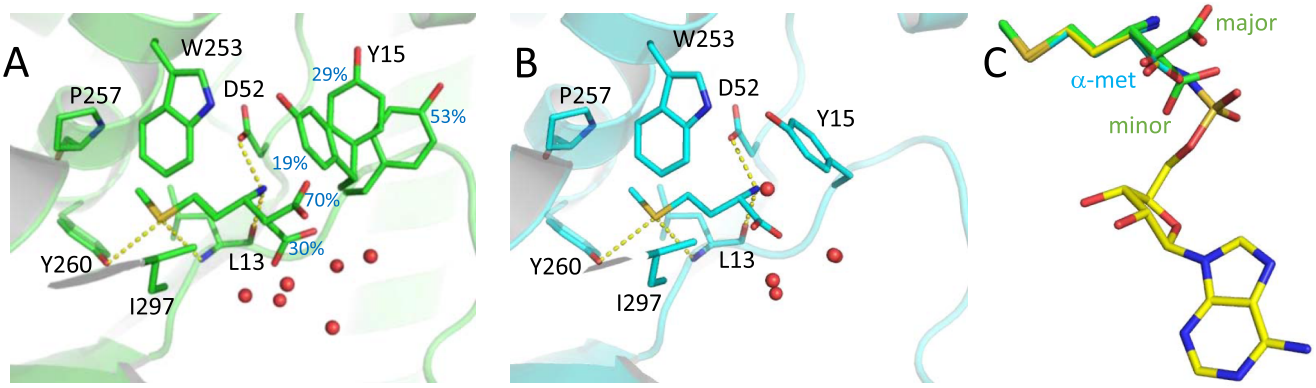


**Fig. 6.** Binding of β³-Met to MetRS (panel A) compared to the binding of α-Met (panel B). Relevant side chains are shown in sticks and nearby water molecules in red spheres. Occupancies of alternative conformations (%) are indicated in blue. MetRS is drawn as a ribbon. The structures of MetRS: β³-Met, MetRS: α-Met (this study) and MetRS:methionyl-sulfamoyl-adenosine (PDBid 1PFY; (Crepin et al., 2003; Larson et al., 2011)) were superimposed. Panel C compares the conformations of the ligands after superimposition. Major and minor conformations of the carboxylate of β³-Met are indicated. Hydrogen bonds are shown with yellow dots. Figs. 5 and 6 were drawn with PyMOL (The PyMOL Molecular Graphics System, Schrödinger, LLC). (For interpretation of the references to colour in this figure legend, the reader is referred to the web version of this article.)

Schmitt et al., 1993) was subcloned into pET15blpa (Guillon et al., 2005) in order to add an N-terminal His-tag to the MetRS product. The QuickChange method (Braman et al., 1996) was used to generate site-directed mutations. The M547 variants were produced in BLR(DE3) cells. Cultures were grown overnight at 37 °C in autoinducible TBAI medium containing 50 μg/mL of ampicillin. The cell pellet was suspended in purification buffer (10 mM Hepes-NaOH pH 7.5, 500 mM NaCl, 3 mM 2-mercaptoethanol) and cells were disrupted by ultrasonic disintegration. After centrifugation, the extract was loaded onto Talon affinity resin (Clontech). The resin was washed with purification buffer containing 10 mM imidazole and the protein eluted by increasing imidazole concentration to 125 mM. The eluate was diluted ten-fold before further purification on a Q-Hiload (GE-Healthcare) ion exchange column. The procedure yielded 15–20 mg of homogeneous protein for a 250 mL culture. Purified proteins were stored either at 4 °C in 10 mM Hepes-NaOH, 10 mM 2-mercaptoethanol or at −20 °C in the same buffer plus 55% glycerol.

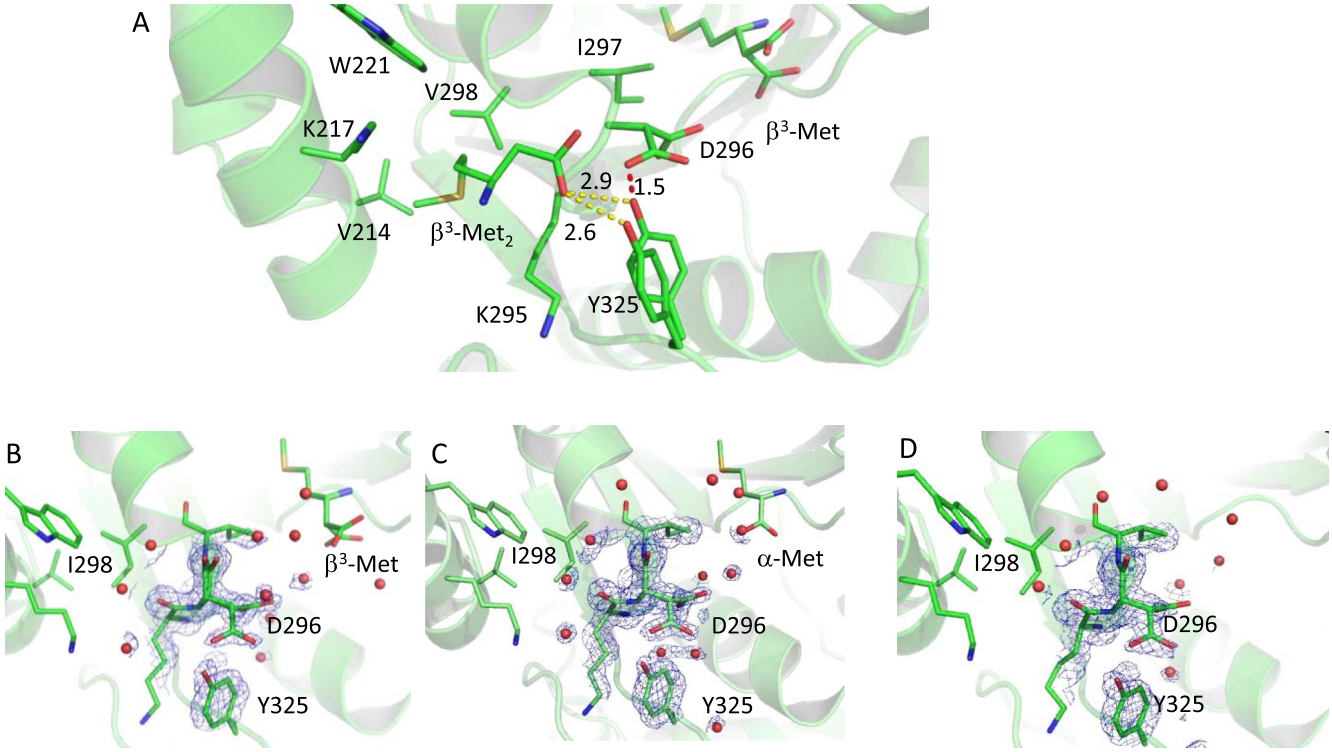


**Fig. 7.** Secondary $\beta^3$-Met binding site ($\beta^3$-$Met_2$) in MetRS. MetRS is shown as a transparent ribbon. Panel A shows the environment of $\beta^3$-$Met_2$. $\beta^3$-Met in the active site is also represented. Relevant side chains are shown in sticks and nearby water molecules in red spheres. The two alternative conformations of D296 and Y325 (see text) are shown. Several distances represented by yellow or red dots are indicated in Å. The bottom panels show the region of D296 in the V298I mutant as a complex with $\beta^3$-Met (panel B), α-Met (panel C) or in the apo form (panel D). The relevant part of the electron density (2mFo-DFc map contoured at 1.0 σ) is represented in blue using the carve command in PyMOL. (For interpretation of the references to colour in this figure legend, the reader is referred to the web version of this article.)

### 3.2. Isotopic [$^{32}$P]PPi-ATP exchange

Amino acid-dependent [$^{32}$P]PPi-ATP exchange activity was measured at 25 °C in standard buffer (20 mM Tris-HCl pH 7.6, 7 mM $MgCl_2$, 10 mM 2-mercaptoethanol, 0.1 mM EDTA) containing 2 mM ATP and 2 mM [$^{32}$P] PPi as described (Blanquet et al., 1974; Schmitt et al., 1994). For Km measurements, concentrations of α-Met or $\beta^3$-Met were varied between 8 μM and 2 mM or 0.125 mM to 8 mM, respectively.

### 3.3. Treatment of $\beta^3$-Met with methionine gamma lyase (MGL)

L-$\beta^3$-Met was purchased from Fluorochem Ltd. (UK), dissolved in standard buffer and adjusted to pH 7.5 with NaOH. For α,γ-elimination of contaminating methionine to α-ketobutyrate, methanethiol and ammonia, 100 μL batches of $\beta^3$-Met (160 mM) were incubated overnight at 37 °C with 1 unit of *Pseudomonas putida* MGL recombinantly expressed in *E. coli* (Biovision Inc., Milpitas, USA) in the presence of 150 μM phosphoenolpyruvate. A control sample was made by omitting MGL; this control treatment had no effect on the rates of [$^{32}$P]PPi-ATP isotopic exchange.

### 3.4. tRNA aminoacylation assay

Aminoacylation of *E. coli* $tRNA_f^{Met}$ produced and purified as described (Mechulam et al., 2007) was assayed using the [3′-$^{32}$P]-labelling method (Ledoux and Uhlenbeck, 2008). $tRNA_f^{Met}$ was labelled by exchange of the 3′ terminal adenosine (Ledoux and Uhlenbeck, 2008) catalyzed by *E. coli* tRNA nucleotidyltransferase overexpressed from a recombinant plasmid (kind gift from Dr. Kozo Tomita, University of Tokyo, Japan). The His-tagged nucleotidyltransferase was purified by affinity on Talon resin. The labelling reaction (50 μL) contained tRNA (1 μM), sodium pyrophosphate (50 μM), MgCl2 (10 mM), glycin (pH 9; 50 mM), [α-$^{32}$P] ATP (0.3 μM, 111 TBq/mmol) and 0.02 μM nucleotidyltransferase. After 5 min at 37 °C, 5 μL of a solution containing 1 μM CTP and 0.1U of pyrophosphatase were added. After 2 min at 37 °C, the reaction was phenol and then ether extracted. The aqueous phase was run over a Micro Bio-Spin P-6 molecular sieving column (Bio-Rad) to remove nucleotides and in particular unreacted ATP. After ethanol precipitation, labelled tRNA was redissolved in standard buffer containing 7 mM $MgCl_2$ and 20 μM unlabelled tRNA.

Aminoacylation activity was measured in 20 μL reactions at 25 °C in 20 mM Tris.HCl (pH 7.6), 7 mM $MgCl_2$, 10 mM 2-mercaptoethanol, 0.1 mM EDTA, 7 mM $MgCl_2$, 150 mM KCl, in the presence of 2 mM ATP, 2 μM [3′-$^{32}$P] $tRNA_f^{Met}$ and 2 mM of either α-Met or MGL-treated $\beta^3$-Met. M547 enzyme diluted in reaction buffer containing 200 μg/mL BSA was used at a concentration of 1 nM in the case of α-Met and 1 μM in the case of $\beta^3$-Met. At desired incubation times, 3 μL of the reaction mixture were withdrawn and mixed with an equal volume of S1 nuclease (NEN from laboratory stocks, 2 units/μl in 0.3 M Na-acetate, pH 4.8). The digestion products were run on a PEI cellulose TLC plate (Bio-Rad) in glacial acetic acid/1 M $NH_4Cl$/water (5:10:85). Plates were phosphorimaged with a Typhoon scanner (GE Healthcare). Images were processed with ImageJ (Schneider et al., 2012) in order to determine for each incubation time the fraction of aminoacylated tRNA, from which aminoacylation rates were derived. A typical experiment is shown in Fig. 5.

### 3.5. Fluorescence at equilibrium

Variations of the intrinsic fluorescence of M547 and its variants (0.5 μM) upon titration with substrates were followed at 25 °C in 20 mM Tris-HCl (pH7.6), 10 mM 2-mercaptoethanol, 2 mM $MgCl_2$ and 0.1 mM EDTA as described (Mechulam et al., 1991; Schmitt et al., 1994). Measurements were done in a Hellma 1 cm × 0.4 cm cuve with

an FP-8300 JASCO spectrofluorometer (λexc = 295 nm, λem = 340 nm). All titration curves were corrected for dilution by multiplying the measured fluorescence by the ratio of the current volume in the cuvette over the initial volume before titration. Concentrations of α-Met or $\beta^3$-Met (untreated or MGL-treated) were varied from 3 μM to 1 mM and from 0.06 mM to 4 mM, respectively. Data were fitted to simple saturation curves from which the corresponding dissociation constants were derived using the Origin software (OriginLab Corp.; see Fig. 2).

### 3.6. Fluorescence at the pre-steady state

Fluorescence measurements at the pre-steady-state were performed as described (Hyafil et al., 1976; Schmitt et al., 1994) using an SX20 stopped flow apparatus (Applied Photophysics, UK). All experiments were performed in 20 mM Tris-HCl (pH 7.6), 10 mM 2-mercaptoethanol, 2 mM $MgCl_2$ and 0.1 mM EDTA. The formation of α- or $\beta^3$-methionyl adenylate was initiated by mixing 1:1 (v/v) an enzyme solution (1 μM for α-Met or 2 μM for $\beta^3$-Met) containing ATP-$Mg^{2+}$ (2 mM) and PPi (10 μM) with a solution containing the same concentrations of ATP-$Mg^{2+}$ plus variable amounts of the amino acid (10 μM to 640 μM for α-Met or 25 μM to 2 mM for $\beta^3$-Met). For the reverse reaction, enzyme:adenylate complexes were pre-formed by incubating the enzyme with ATP-$Mg^{2+}$ and the amino acid for a few minutes at 25 °C (1 μM enzyme, 0.1 mM ATP-$Mg^{2+}$ and 500 μM α-Met or 2 μM enzyme, 2 mM ATP-$Mg^{2+}$ and 25 μM $\beta^3$-Met). The solution was then mixed 1:1 (v/v) with a solution containing the same concentrations of ATP-$Mg^{2+}$ and amino acid plus variable amounts of pyrophosphate (20 μM to 1.28 mM for α-Met or 20 μM to 2 mM for $\beta^3$-Met). After mixing, fluorescence was recorded and fitted to single exponentials from which the rate constants were derived (Supplementary Fig. S1). Each rate was determined three times. Kinetic parameters ($k_f$ and $k_b$, see Scheme 1) and equilibrium parameters ($K_{Met}^{ATP}$ and $K_{PP}$) were deduced from the fit of the measured rate constants to the theoretical saturation curves (Hyafil et al., 1976; Mechulam et al., 1991; Schmitt et al., 1994) using Origin. Each experiment was performed at least twice independently. Results in Table 1 are expressed as mean ± either standard deviation from the independent experiments or standard error from the fitting procedure, whichever the greater. All experiments were performed using MGL-treated $\beta^3$-Met.

### 3.7. Preparation of samples for mass spectrometry experiments

Amino acid samples (160 mM α-Met, β-Met or MGL-treated β-Met) were acidified by adding formic acid (10% v/v final concentration). Samples were then diluted 1000-fold in 0.1% formic acid prior to analysis. Aminoacyl adenylate samples were prepared in 0.8 mL solutions (20 mM Tris-HCl pH 7.6, 2 mM $MgCl_2$, 10 mM 2-mercaptoethanol, 0.1 mM EDTA) containing 0.5 μM MetRS, 1 mM MGL-treated β-Met and 2 mM ATP-$Mg^{2+}$. The reaction at 25 °C was monitored by following the fluorescence as described above. After *ca* 15 min, reaction was nearly complete and 10% (v/v) formic acid and precipitated material was removed by centrifugation prior to analysis. Analysis of tRNA aminoacylation after S1 nuclease digestion was performed essentially as described (Hartman et al., 2007, 2006). $tRNA_f^{Met}$ was first aminocylated in 1 mL samples containing 20 mM Tris-HCl (pH 7.6), 7 mM $MgCl_2$, 10 mM 2-mercaptoethanol, 0.1 mM EDTA, 2 mM ATP, 1 μM MetRS and either 0.4 mM of α-Met of 1 mM of β-Met. After incubation for 30 min at 25 °C, the reaction was divided into 4 samples each of which was precipitated with ethanol. One sample was dissolved in 100 μL of 3 mM Na-acetate (pH 5.5) containing 1 mM zinc acetate and tRNA was digested with 10 units of S1 nuclease for 20 min at 37 °C. Formic acid (10% v/v final concentration) was then added before mass spectrometry analysis. Another sample was submitted to acetylation as follows. After dissolution of the pellet in 100 μL of 5 mM sodium acetate (pH 5.5), 100 μL DMSO, 20 μL of glacial acetic acid and 20 μL of acetic anhydride were added. After a 30 min incubation on ice, the solution was ethanol precipitated and tRNA was digested with S1 nuclease, as described above.

### 3.8. Mass spectrometry

Chromatographic grade solvents (99.99% purity), acetonitrile (ACN) and formic acid (FA), were purchased from Sigma Aldrich. Liquid chromatography/ high-resolution mass spectrometry (LC-HRMS) analyses were performed with the timsTOF mass spectrometer coupled with an Elute HPLC system (Bruker Daltonics, Bremen, Germany).

For all experiments, 10 μL of the sample were injected and separated on an Atlantis T3 column (3 μm, 150 × 2.1 mm; Waters, Saint Quentin, France). The effluent was introduced at a flow rate of 0.2 mL $min^{-1}$ into the interface with a gradient increasing from 10% of solvent B to 90% in 8 min to achieve 100% at 10 min (A: water with 0.1% formic acid (FA); B: acetonitrile with 0.1% FA). From 10 min to 12 min, the percentage of solvent increased until 90%. The gradient was then set at 10% of B for the last 6 min.

Electrospray ionization was operated in the positive ion mode. Capillary and end plate voltages were set at −4.5 kV and −0.5 kV, respectively. Nitrogen was used as the nebulizer and drying gas at 2 bar and 8 L/min, respectively, with a drying temperature of 220 °C.

In MS/MS experiments, the precursor ion was selected with an isolation window of 1 Da and the collision induced dissociation was performed using collision energies ($E_{col}$) ranging from 7 to 25 eV. Tuning mix (Agilent, France) was used for calibration. The elemental compositions of all ions were determined with the instrument software Data Analysis. The precision of mass measurement was better than 5 ppm.

### 3.9. Crystallization and structure determination

Crystals of M547 or of its variants were obtained in a solution containing 30 mM $KPO_4$, 4 mM 2-mercaptoethanol, 1.08 mM ammonium citrate (pH 7.0) and 3.6 mg/mL of protein by microseeding with crystals of M547 (Mechulam et al., 1999b). For ligand binding studies, the amino acid was added to the crystallization medium prior to microseeding. Final concentrations during crystallization were 2 mM for α-Met or 20 mM for $\beta^3$-Met. For data collection, crystals were quickly soaked in a solution containing 1.4 M ammonium citrate, 30 mM potassium phosphate (pH 7.0) and 25% v/v of glycerol before flash-cooling in liquid nitrogen. Data were collected at the Proxima 1 and Proxima 2 beamlines at SOLEIL synchrotron (Gif sur Yvette, France). Diffraction images were analyzed with the XDS program (Kabsch, 1988; Collaborative Computational Project n°4, 1994) and the data further processed using programs from the CCP4 package (Collaborative Computational Project n°4, 1994). Data statistics are summarized in Table 1. Each structure was solved by rigid body refinement of the M551 model (PDB id 1QQT), using PHENIX (Adams et al., 2010). Coordinates and associated B factors were refined through several cycles of manual adjustments with Coot (Emsley et al., 2010) and positional refinement with PHENIX. Refinement statistics are summarized in Table 1.

## 4. Accession numbers

Models coordinates and reflection files were deposited at the PDB with identification numbers 6SPN (MetRS-$\beta^3$Met), 6SPO (MetRS-αMet), 6SPP (MetRS_V298I), 6SPQ (MetRS_V298I-αMet), 6SPR (MetRS_V298I-$\beta^3$Met).

## CRediT authorship contribution statement

**Giuliano Nigro**: Investigation, Methodology, Writing - review & editing. Sophie Bourcier: Investigation, Methodology, Writing - review

& editing. **Christine Lazennec-Schurdevin**: Investigation, Writing - review & editing. **Emmanuelle Schmitt**: Conceptualization, Methodology, Supervision, Writing - original draft, Writing - review & editing. **Philippe Marlière**: Conceptualization, Methodology, Supervision, Writing - review & editing. **Yves Mechulam**: Conceptualization, Methodology, Supervision, Writing - original draft, Writing - review & editing.

## Declaration of Competing Interest

The authors declare that they have no known competing financial interests or personal relationships that could have appeared to influence the work reported in this paper.

## Acknowledgements

This work was supported by grants from the Centre National de la Recherche Scientifique (France) and by Ecole polytechnique (France) to Unité Mixte de Recherche n°7654. GN was a recipient of a PhD scholarship from Ecole polytechnique. We thank the staff of the macromolecular crystallography PX1 and PX2 beamlines at the SOLEIL synchrotron (Saclay, France) for expert assistance during data collection. Kozo Tomita (University of Tokyo, Japan) is acknowledged for the kind gift of the *E. coli* tRNA nucleotidyltransferase-overproducing plasmid.

## Appendix A. Supplementary data

Supplementary data to this article can be found online at https://doi.org/10.1016/j.jsb.2019.107435.

## References

Adams, P.D., Afonine, P.V., Bunkóczi, G., Chen, V.B., Davis, I.W., Echols, N., Headd, J.J., Hung, L.-W., Kapral, G.J., Grosse-Kunstleve, R.W., McCoy, A.J., Moriarty, N.W., Oeffner, R., Read, R.J., Richardson, D.C., Richardson, J.S., Terwilliger, T.C., Zwart, P.H., 2010. PHENIX: a comprehensive Python-based system for macromolecular structure solution. Acta Crystallogr. Section D, Biol. Crystallogr. 66, 213–221.

Blanquet, S., Fayat, G., Waller, J.P., 1974. The mechanism of action of methionyl-tRNA synthetase fromEscherichia coli. Mechanism of the amino-acid activation reaction catalyzed by the native and the trypsin-modified enzymes. Eur. J. Biochem. 44, 343–351.

Blanquet, S., Fayat, G., Poiret, M., Waller, J.P., 1975. The mechanism of action of methionyl-tRNA synthetase from Escherichia coli. Inhibition by adenosine and 8-aminoadenosine of the amino-acid activation reaction. Eur. J. Biochem. 51, 567–571.

Braman, J., Papworth, C., Greener, A., 1996. Site-directed mutagenesis using double-stranded plasmid DNA templates. Methods Mol. Biol. (Clifton, N.J.) 57, 31–44. https://doi.org/10.1385/0-89603-332-5:31.

Brick, P., Bhat, T.N., Blow, D.M., 1989. Structure of tyrosyl-tRNA synthetase refined at 2.3 Å resolution. Interaction of the enzyme with the tyrosyl adenylate intermediate. J. Mol. Biol. 208, 83–98.

Cheloha, R.W., Sullivan, J.A., Wang, T., Sand, J.M., Sidney, J., Sette, A., Cook, M.E., Suresh, M., Gellman, S.H., 2015. Consequences of periodic alpha-to-beta(3) residue replacement for immunological recognition of peptide epitopes. ACS Chem. Biol. 10, 844–854. https://doi.org/10.1021/cb500888q.

Chin, J.W., 2017. Expanding and reprogramming the genetic code. Nature 550, 53–60. https://doi.org/10.1038/nature24031.

Collaborative Computational Project n°4, 1994. The CCP4 suite: programs from protein crystallography. Acta Cristallogr. D50, 760–763.

Crepin, T., Schmitt, E., Mechulam, Y., Sampson, P.B., Vaughan, M.D., Honek, J.F., Blanquet, S., 2003. Use of analogues of methionine and methionyl adenylate to sample conformational changes during catalysis in Escherichia coli methionyl-tRNA synthetase. J. Mol. Biol. 332, 59–72. https://doi.org/10.1016/S0022-2836(03)00917-3.

Dedkova, L.M., Fahmi, N.E., Paul, R., del Rosario, M., Zhang, L., Chen, S., Feder, G., Hecht, S.M., 2011. β-Puromycin selection of modified ribosomes for in vitroincorporation of β-amino acids. Biochemistry 51, 401–415. https://doi.org/10.1021/bi2016124.

Emsley, P., Lohkamp, B., Scott, W.G., Cowtan, K., 2010. Features and development of Coot. Acta Crystallogr. D66, 486–501.

Fayat, G., Fromant, M., Blanquet, S., 1977. Couplings between the sites for methionine and adenosine 5'-triphosphate in the amino acid activation reaction catalyzed by trypsin-modified methionyl-transfer RNA synthetase from Escherichia coli. Biochemistry 16, 2570–2579.

Fersht, A.R., 1987. Dissection of the structure and activity of the tyrosyl-tRNA synthetase by site-directed mutagenesis. Biochemistry 26, 8031–8037.

Fersht, A.R., Dingwall, C., 1979. An editing mechanism for the methionyl-tRNA synthetase in the selection of aminoacids in protein synthesis. Biochemistry 18, 1250–1256.

Fujino, T., Goto, Y., Suga, H., Murakami, H., 2016. Ribosomal synthesis of peptides with multiple beta-amino acids. J. Am. Chem. Soc. 138, 1962–1969. https://doi.org/10.1021/jacs.5b12482.

Fukumoto, M., Kudou, D., Murano, S., Shiba, T., Sato, D., Tamura, T., Harada, S., Inagaki, K., 2014. The role of amino acid residues in the active site of L-methionine γ-lyase from pseudomonas putida. Biosci. Biotechnol. Biochem. 76, 1275–1284. https://doi.org/10.1271/bbb.110906.

Guillon, L., Schmitt, E., Blanquet, S., Mechulam, Y., 2005. Initiator tRNA binding by e/aIF5B, the eukaryotic/archaeal homologue of bacterial initiation factor IF2. Biochemistry 44, 15594–15601. https://doi.org/10.1021/bi051514j.

Hartman, M.C.T., Josephson, K., Szostak, J.W., 2006. Enzymatic aminoacylation of tRNA with unnatural amino acids. PNAS 103, 4356–4361. https://doi.org/10.1073/pnas.0509219103.

Hartman, M.C.T., Josephson, K., Lin, C.-W., Szostak, J.W., 2007. An expanded set of amino acid analogs for the ribosomal translation of unnatural peptides. PLoS One 2, e972–15. https://doi.org/10.1371/journal.pone.0000972.

Heck, T., Limbach, M., Geueke, B., Zacharias, M., Gardiner, J., Kohler, H.-P.E., Seebach, D., 2006. Enzymatic degradation of beta- and mixed alpha, beta-oligopeptides. Chem. Biodivers. 3, 1325–1348. https://doi.org/10.1002/cbdv.200690136.

Hyafil, F., Jacques, Y., Fayat, G., Fromant, M., Dessen, P., Blanquet, S., 1976. Methionyl-tRNA synthetase from Escherichia coli: active stoichiometry and stopped-flow analysis of methionyl adenylate formation. Biochemistry 15, 3678–3685.

Johnson, J.A., Lu, Y.Y., Van Deventer, J.A., Tirrell, D.A., 2010. Residue-specific incorporation of non-canonical amino acids into proteins: recent developments and applications. Curr. Opin. Chem. Biol. 14, 774–780. https://doi.org/10.1016/j.cbpa.2010.09.013.

Kabsch, W.J., 1988. Evaluation of single crystal X-ray diffraction data from a position sensitive detector. J. Appl. Crystallogr. 21, 916–924.

Karplus, P.A., Diederichs, K., 2012. Linking crystallographic model and data quality. Science (New York, N.Y.) 336, 1030–1033. https://doi.org/10.1126/science.1218231.

Katoh, T., Suga, H., 2018. Ribosomal incorporation of consecutive beta-amino acids. J. Am. Chem. Soc. 140, 12159–12167. https://doi.org/10.1021/jacs.8b07247.

Larson, E.T., Kim, J.E., Zucker, F.H., Kelley, A., Mueller, N., Napuli, A.J., Verlinde, C.L.M.J., Fan, E., Buckner, F.S., Van Voorhis, W.C., Merritt, E.A., Hol, W.G.J., 2011. Structure of Leishmania major methionyl-tRNA synthetase in complex with intermediate products methionyladenylate and pyrophosphate. Biochimie 93, 570–582. https://doi.org/10.1016/j.biochi.2010.11.015.

Ledoux, S., Uhlenbeck, O.C., 2008. [3′-32P]-labeling tRNA with nucleotidyltransferase for assaying aminoacylation and peptide bond formation. Methods 44, 74–80. https://doi.org/10.1016/j.ymeth.2007.08.001.

Liu, C.C., Schultz, P.G., 2010. Adding new chemistries to the genetic code. Annu. Rev. Biochem. 79, 413–444. https://doi.org/10.1146/annurev.biochem.052308.105824.

Mahdavi, A., Hamblin, G.D., Jindal, G.A., Bagert, J.D., Dong, C., Sweredoski, M.J., Hess, S., Schuman, E.M., Tirrell, D.A., 2016. Engineered aminoacyl-tRNA synthetase for cell-selective analysis of mammalian protein synthesis. J. Am. Chem. Soc. 138, 4278–4281. https://doi.org/10.1021/jacs.5b08980.

Maini, R., Nguyen, D.T., Chen, S., Dedkova, L.M., Chowdhury, S.R., Alcala-Torano, R., Hecht, S.M., 2013. Incorporation of β-amino acids into dihydrofolate reductase by ribosomes having modifications in the peptidyltransferase center. Bioorg. Med. Chem. 21, 1088–1096. https://doi.org/10.1016/j.bmc.2013.01.002.

Mechulam, Y., Dardel, F., Le Corre, D., Blanquet, S., Fayat, G., 1991. Lysine 335, part of the KMSKS signature sequence, plays a crucial role in the amino acid activation catalysed by the methionyl-tRNA synthetase from Escherichia coli. J. Mol. Biol. 217, 465–475.

Mechulam, Y., Schmitt, E., Maveyraud, L., Zelwer, C., Nureki, O., Yokoyama, S., Konno, M., Blanquet, S., 1999. Crystal structure of Escherichia coli methionyl-tRNA synthetase highlights species-specific features. J. Mol. Biol. 294, 1287–1297. https://doi.org/10.1006/jmbi.1999.3339.

Mechulam, Y., Guillon, L., Yatime, L., Blanquet, S., Schmitt, E., 2007. Protection-based assays to measure aminoacyl-tRNA binding to translation initiation factors. Methods Enzymol. 430, 265–281. https://doi.org/10.1016/S0076-6879(07)30011-6.

Mellot, P., Mechulam, Y., Le Corre, D., Blanquet, S., Fayat, G., 1989. Identification of an amino acid region supporting specific methionyl-tRNA synthetase: tRNA recognition. J. Mol. Biol. 208, 429–443.

Melo Czekster, C., Robertson, W.E., Walker, A.S., Söll, D., Schepartz, A., 2016. In vivo biosynthesis of a β-amino acid-containing protein. J. Am. Chem. Soc. 138, 5194–5197. https://doi.org/10.1021/jacs.6b01023.

Murakami, H., Kourouklis, D., Suga, H., 2003. Using a solid-phase ribozyme aminoacylation system to reprogram the genetic code. Chem. Biol. 10, 1077–1084.

Murakami, H., Ohta, A., Ashigai, H., Suga, H., 2006. A highly flexible tRNA acylation method for non-natural polypeptide synthesis. Nat. Methods 3, 357–359. https://doi.org/10.1038/nmeth877.

Ngo, J.T., Champion, J.A., Mahdavi, A., Tanrikulu, I.C., Beatty, K.E., Connor, R.E., Yoo, T.H., Dieterich, D.C., Schuman, E.M., Tirrell, D.A., 2009. Cell-selective metabolic labeling of proteins. Nat. Chem. Biol. 5, 715–717.

Ohuchi, M., Murakami, H., Suga, H., 2007. The flexizyme system: a highly flexible tRNA aminoacylation tool for the translation apparatus. Curr. Opin. Chem. Biol. 11, 537–542. https://doi.org/10.1016/j.cbpa.2007.08.011.

Petersson, E.J., Schepartz, A., 2008. Toward beta-amino acid proteins: design, synthesis, and characterization of a fifteen kilodalton beta-peptide tetramer. J. Am. Chem. Soc. 130, 821–823. https://doi.org/10.1021/ja077245x.

Petersson, E.J., Craig, C.J., Daniels, D.S., Qiu, J.X., Schepartz, A., 2007. Biophysical characterization of a beta-peptide bundle: comparison to natural proteins. J. Am.

Chem. Soc. 129, 5344–5345. https://doi.org/10.1021/ja070567g.
Schmitt, E., Meinnel, T., Panvert, M., Mechulam, Y., Blanquet, S., 1993. Two acidic residues ofEscherichia colimethionyl-tRNA synthetase are negative discriminants towards the binding of non-cognate tRNA anticodons. J. Mol. Biol. 233, 615–628.
Schmitt, E., Meinnel, T., Blanquet, S., Mechulam, Y., 1994. Methionyl-tRNA synthetase needs an intact and mobile 332KMSKS336 motif in catalysis of methionyl adenylate formation. J. Mol. Biol. 242, 566–577.
Schmitt, E., Moulinier, L., Fujiwara, S., Imanaka, T., Thierry, J.C., Moras, D., 1998. Crystal structure of aspartyl-tRNA synthetase from Pyrococcus kodakaraensisKOD: archaeon specificity and catalytic mechanism of adenylate formation. EMBO J. 17, 5227–5237.
Schmitt, E., Tanrikulu, I.C., Yoo, T.H., Panvert, M., Tirrell, D.A., Mechulam, Y., 2009. Switching from an induced-fit to a lock-and-key mechanism in an aminoacyl-tRNA synthetase with modified specificity. J. Mol. Biol. 394, 843–851. https://doi.org/10.1016/j.jmb.2009.10.016.
Schneider, C.A., Rasband, W.S., Eliceiri, K.W., 2012. NIH Image to ImageJ: 25 years of image analysis. Nat. Methods 9, 671–675.
Seebach, D., Gardiner, J., 2008. Beta-peptidic peptidomimetics. Acc. Chem. Res. 41, 1366–1375. https://doi.org/10.1021/ar700263g.
Seebach, D., Hook, D.F., Glattli, A., 2006. Helices and other secondary structures of beta- and gamma-peptides. Biopolymers 84, 23–37. https://doi.org/10.1002/bip.20391.
Serre, L., Verdon, G., Choinowski, T., Hervouet, N., Risler, J.L., Zelwer, C., 2001. How methionyl-tRNA synthetase creates its amino acid recognition pocket upon L-methionine binding. J. Mol. Biol. 306, 863–876. https://doi.org/10.1006/jmbi.2001.4408.
Shimizu, Y., Inoue, A., Tomari, Y., Suzuki, T., Yokogawa, T., Nishikawa, K., Ueda, T., 2001. Cell-free translation reconstituted with purified components. Nat. Biotechnol. 19, 751–755.
Tanrikulu, I.C., Schmitt, E., Mechulam, Y., Goddard, W.A., Tirrell, D.A., 2009. Discovery of Escherichia coli methionyl-tRNA synthetase mutants for efficient labeling of proteins with azidonorleucine in vivo. Proc. Natl. Acad. Sci. U.S. A. 106, 15285–15290. https://doi.org/10.1073/pnas.0905735106.
Wang, L., Xie, J., Schultz, P.G., 2006. Expanding the genetic code. Annu. Rev. Biophys. Biomol. Struct. 35, 225–249. https://doi.org/10.1146/annurev.biophys.35.101105.121507.
Webb, A.I., Dunstone, M.A., Williamson, N.A., Price, J.D., de Kauwe, A., Chen, W., Oakley, A., Perlmutter, P., McCluskey, J., Aguilar, M.-I., Rossjohn, J., Purcell, A.W., 2005. T cell determinants incorporating beta-amino acid residues are protease resistant and remain immunogenic in vivo. J. Immunol. 175, 3810–3818. https://doi.org/10.4049/jimmunol.175.6.3810.